In Situ NMR and Electrochemical Quartz Crystal Microbalance Reveal the Structure of the Electric Double-Layer in Supercapacitor Electrodes

John M. Griffin,[1] Alexander C. Forse,[1]

Wan-Yu Tsai,[3,4] Pierre-Louis Taberna,[3,4] Patrice Simon,[3,4] and Clare P. Grey[1,2]*

[1]*Department of Chemistry, University of Cambridge, Lensfield Road, Cambridge, CB2 1EW, UK*

[2]*Department of Chemistry, Stony Brook University, Stony Brook, New York, 11794-3400, United States*

[3]*Université Paul Sabatier Toulouse III, CIRIMAT, UMR-CNRS 5085, F-31062 Toulouse, France*

[4]*Réseau sur le Stockage Electrochimique de l'Energie (RS2E), FR CNRS 3459, France*

email cpg27@cam.ac.uk

Submitted to Nature Materials (Article format)

Abstract

Supercapacitors store charge through the electrosorption of ions on microporous electrodes. Despite major efforts to understand this phenomenon, a molecular-level picture of the electric double-layer in working devices is still lacking as few techniques can selectively observe the ionic species at the electrode-electrolyte interface. Here, we use *in situ* NMR to directly quantify the populations of anionic and cationic species within a working microporous carbon supercapacitor electrode. Our results show that charge storage mechanisms for the electrolyte studied are different for positively- and negatively-polarized electrodes for the electrolyte tetraethylphosphonium tetrafluoroborate in acetonitrile; for positive polarization charging proceeds by ion exchange, whereas for negative polarization, counter-ion adsorption dominates. *In situ* electrochemical quartz crystal microbalance (EQCM) measurements support the NMR results and indicate that adsorbed ions are only partially solvated. These results provide new molecular-level insight, the methodology offering exciting possibilities for the study of pore/ion size, desolvation and other effects on charge storage in supercapacitors.

Introduction

The mechanism of charge storage in supercapacitors has traditionally been attributed to the electrosorption of ions on the surface of a charged electrode to form an electric double-layer. However, in recent years a number of empirical observations have shown that the mechanism is more complex, with factors such as relative pore/ion sizes[1-3] and desolvation effects[4,5] playing important roles. Theoretical studies have led the way in understanding supercapacitor charging on the molecular level,[6,7] and have demonstrated that charge screening,[8-10] ionic rearrangement[11] and confinement,[12] and pore surface properties[13] can have significant effects on the capacitance and charging dynamics. Nevertheless, theoretical simulations necessarily depend on assumptions and simplifications, and many questions concerning details of the charging mechanisms in real devices remain unanswered. In particular, it is not clear if charging is a purely adsorptive process, or if ion exchange and expulsion from the charged electrodes also contribute to the formation of the electric double-layer. Recently, *in situ* experimental methodologies based on electrochemical quartz crystal microbalance (EQCM)[14,15] and *infra*-red (IR) spectroscopy[16,17] have started to address these questions. These methods can observe ion adsorption and expulsion in charged electrodes, and have been able to distinguish purely adsorptive regimes from ion mixing during charging. However, neither of these techniques alone permit the direct quantification of species within the electric double-layer in absolute terms, EQCM measuring total mass changes in the electrode and IR spectroscopy measuring only the

ions outside of the pores, and so an unambiguous picture of the charging mechanism has not yet been obtained.

One approach that has recently shown promise for the study of supercapacitors is nuclear magnetic resonance (NMR) spectroscopy. NMR has the advantage that it is element selective, thereby allowing individual ionic species to be observed independently.[18,19] *Ex situ* NMR measurements on disassembled supercapacitor electrodes have revealed changes in the populations and local environments of ionic species that result from charging.[20] *In situ* NMR and magnetic resonance imaging methods have also been developed, which allow changes in the local environments of the ions in the electric double layer to be observed for working devices.[21-24] These approaches have provided qualitative insight into the charging mechanism for a range of electrolyte systems. However, in principle NMR is fully quantitative and should enable the measurement of absolute ion populations at the electrode-electrolyte interface. In particular, the combination of NMR with EQCM, which tracks the displacement of all electrolyte species including solvent molecules, should provide a full description of the structure of the electric-double layer.

Here, we use tetraethylphosphonium tetrafluoroborate (PEt_4-BF_4) salt dissolved in acetonitrile (ACN) as the electrolyte, employing ^{31}P and ^{19}F NMR experiments to enable the selective observation of the PEt_4 cations and BF_4 anions, respectively. Deuterated ACN was also used to enable the observation of solvent species by ^{2}H NMR (as described in Supplementary Information). Experiments have been performed on commercial YP-50F activated carbon, for which gas sorption measurements show an average pore size of 0.9 nm with 92% of pores being smaller than 2 nm. The specific surface area is 1730 $m^2 \cdot g^{-1}$ and the total pore volume is 0.75 $cm^3 \cdot g^{-1}$ (see Supplementary Information).

Results

Supercapacitor bag cells were constructed following a shifted 'overlaid' design, allowing a single electrode to be studied independently inside the NMR coil whilst maintaining good capacitive properties.[24] Electrodes were fabricated using 95 wt% YP-50F and 5 wt% PTFE binder (see Materials and Methods). Fig. 1 shows ^{31}P and ^{19}F NMR spectra of individual supercapacitor electrodes in cells held at 0 V with electrolyte concentrations of 1.5 M, 0.75 M and 0.5 M. In each spectrum, intense 'ex-pore' resonances are observed at 40 ppm (^{31}P) and –150 ppm (^{19}F), corresponding to ions located in voids between carbon particles and in electrolyte that resides in a small reservoir between the two electrodes. Small features visible in the ex-pore

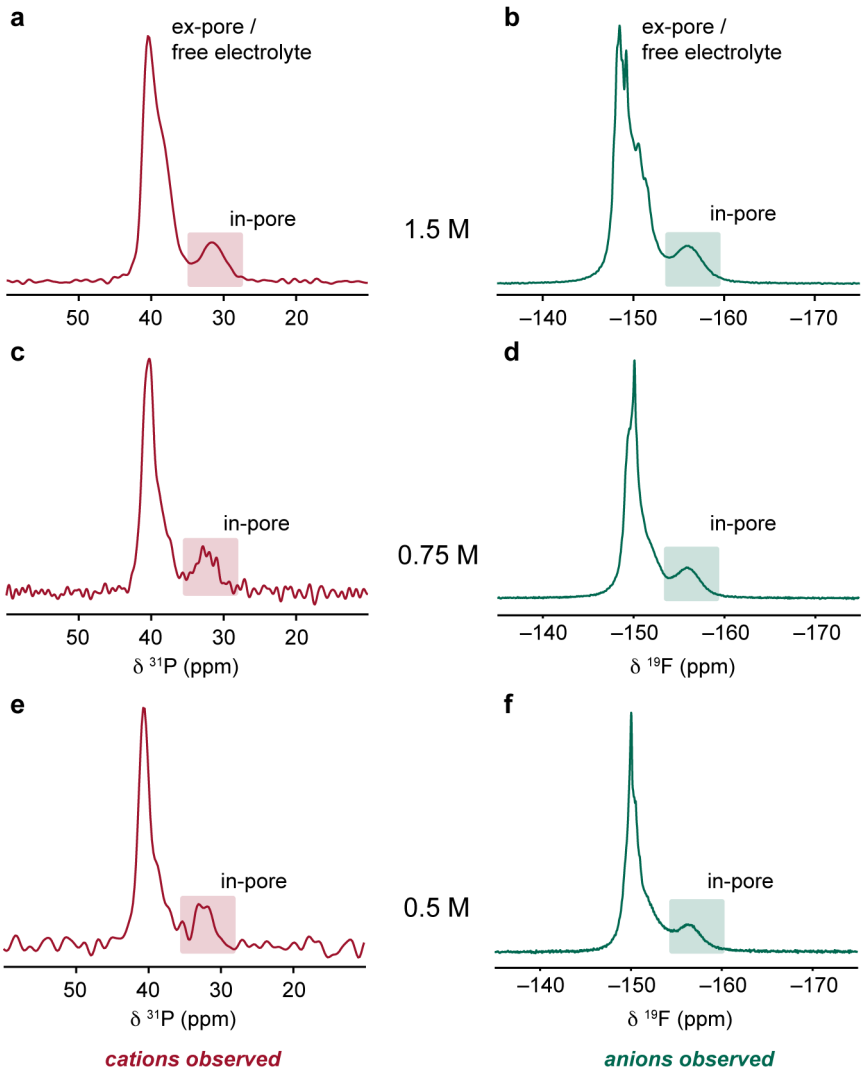

Figure 1. ^{31}P (a, c, e) and ^{19}F (b, d, f) NMR spectra of individual supercapacitor electrodes showing in- and ex-pore cation and anion environments. Electrolyte concentrations are (a, b) 1.5 M, (c, d) 0.75 M and (e, f) 0.5 M. Supercapacitors were held at a cell voltage of 0 V. The in-pore resonances in each spectrum are highlighted.

resonances are due to susceptibility effects associated with the bag cell components and geometric anisotropy of the cell.[21,22] Weaker 'in-pore' resonances corresponding to ions inside the micropores close to carbon surfaces are also observed, shifted to lower frequency by 5 - 7 ppm. The shift of the in-pore resonance from that of the ex-pore resonance is due to diamagnetic nucleus independent chemical shift (NICS) effects (often referred to as 'ring current' effects) associated with the delocalized electrons in the predominantly sp^2-bonded carbon surface.[22,25] Calculations indicate that the NICS effect should be significant for species within a few Ångstroms from the carbon surface. However, the effects of dynamics must also be considered as fast exchange between different positions within a pore will result in an averaging of the observed chemical shift. Taking this into account, NICS values of around 5 ppm have been predicted for species inside pores up to 2 nm in width, consistent with the shifts observed here.[25]

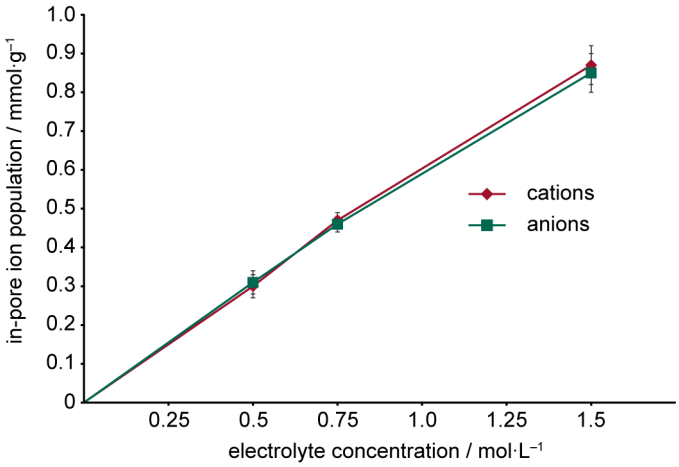

Figure 2. In-pore ion populations per gram of YP-50F at 0 V plotted as a function of concentration for PEt_4-BF_4 / ACN electrolyte. For each concentration equal populations of cations and anions are adsorbed and the total in-pore ion population varies approximately linearly with electrolyte concentration.

Through comparison of the in-pore resonance intensities with calibration samples, it is possible to quantify the number of in-pore species in absolute terms and gain insight into the adsorption properties. In-pore ion populations are plotted as a function of electrolyte concentration in Fig. 2. For the three electrolyte concentrations studied, in-pore anion and cation populations at 0 V are balanced and vary approximately linearly with the concentration. Using estimated solvated ion diameters of 1.35 nm (PEt_4^+) and 1.16 nm (BF_4^-)[26] (see Supplementary Information) and the measured ion uptakes at 0 V, we find that the in-pore ions should occupy a total volume of 1.12 cm^3 (1.5 M electrolyte), 0.56 cm^3 (0.75 M electrolyte) and 0.37 cm^3 (0.5 M electrolyte) per gram of YP-50F. For the 1.5 M electrolyte, the total volume of the in-pore ions estimated on this basis is *significantly* larger than the total pore volume of 0.75 $cm^3 \cdot g^{-1}$ for YP-50F. This indicates that for this concentration, the assumption of each ion having a complete ACN solvation shell is not valid; instead, the ions must be more densely packed inside the micropores, with partial desolvation or overlap of their solvation shells.

To investigate changes in the in-pore ion behaviour during charging, *in situ* NMR experiments were performed as the supercapacitor cells were charged sequentially from total cell voltages of 0 to 1.5 V in steps of 0.25 V. They were then discharged in a single step to 0 V, before being charged in steps of –0.25 V to –1.5 V. ^{19}F and ^{31}P *in situ* NMR spectra were acquired at each voltage (Fig. 3) after cells had been held for 60 minutes (1.5 M & 0.75 M electrolyte) or 90 minutes (0.5 M electrolyte), until a negligible constant residual current was obtained (see Supplementary Information). In both voltage ranges, the in-pore cation and anion resonances move to higher frequency in the NMR spectra as the cells are charged. This is consistent with previous results[21,22] and is due to changes in the nucleus-independent chemical shifts (NICS) that result from the electronic charge that is developed within the carbon electrode: charging of π-bonded

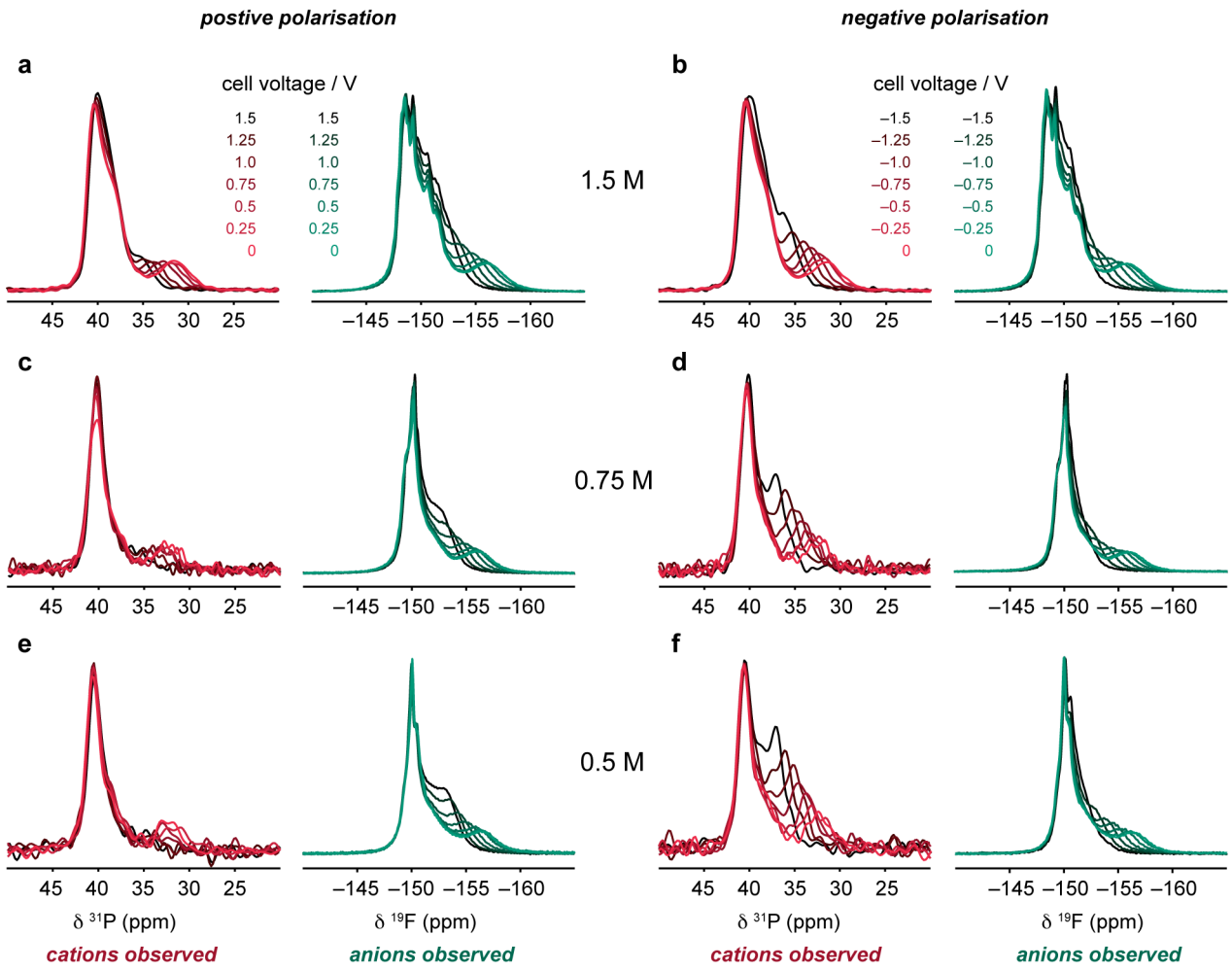

Figure 3. *In situ* ^{31}P and ^{19}F NMR spectra of individual supercapacitor electrodes at different states of charge. Spectra recorded in the range 0 → 1.5 V are shown in (a, c, e); spectra recorded in the range 0 → –1.5 V are shown in (b, d, f). Electrolyte concentrations are (a, b) 1.5 M, (c, d) 0.75 M and (e, f) 0.5 M. In-pore anion intensities increase for positive charging, while in-pore cation intensities increase for negative charging.

carbon systems gives rise to so-called paratropic or anti-aromatic ring currents, which result in positive NICS for nearby species.[22]

While the frequencies of the in-pore resonances depend on the electronic charge state of the electrode surface, importantly, the intensities of the in-pore resonances correspond to the number of in-pore ions within the electrode. As the cell potentials are varied, changes in the in-pore resonance intensities reflect the changing ion populations within the electric double-layer that is formed at the electrode-electrolyte interface within the micropores. In the positive voltage range, the in-pore resonances in the ^{19}F NMR spectra increase in intensity as the cell is charged, showing that anions are absorbed into the micropores during charging. For the negative voltage range, an increase in the in-pore cation population is observed in the ^{31}P NMR spectra as cations are absorbed into the micropores. These results provide a qualitative picture that is consistent with the

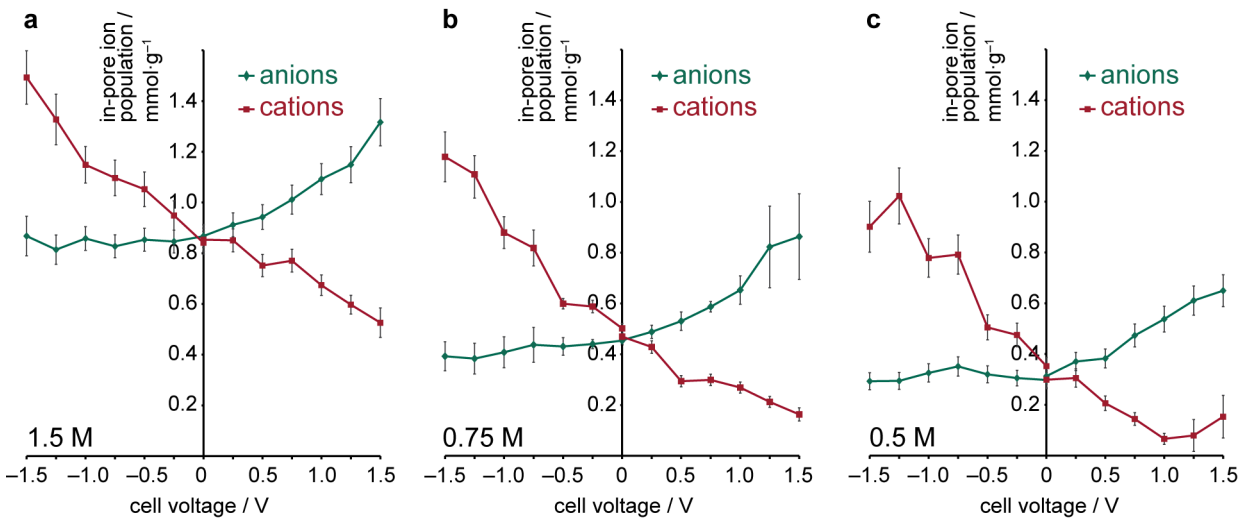

Figure 4. In-pore ion populations for supercapacitor electrodes at different charges states in the range –1.5 to +1.5 V with (a) 1.5 M, (b) 0.75 M and (c) 0.5 M electrolyte concentrations. Values are given as milimoles per gram of YP-50F carbon in a single electrode. Lines joining the data points are a guide to the eye. Ion exchange is observed for positive charging whereas cation adsorption dominates for negative charging.

accepted view of supercapacitor charging: as electronic charge accumulates within the electrode, ions of opposite charge are adsorbed onto the surface to form an electric double-layer.

Absolute ion populations determined from the deconvoluted in-pore resonance intensities, plotted in Fig. 4, offer more quantitative insight and provide a detailed compositional picture of the electric double-layer during charging. Interestingly, for the positive cell voltage range, we find that the charging mechanism is *not* a purely adsorptive process. For all electrolyte concentrations, the in-pore anion population increases together with a simultaneous decrease in the in-pore cation population. This shows that charge storage is actually driven by ion exchange, whereby anions are absorbed into the micropores while cations are simultaneously ejected. This leads to an overall negative ionic charge, which forms an electric double-layer with the positive electronic charge that accumulates on the electrode surface. Over the voltage range studied, the number of cations ejected from the micropores is approximately equal to the number of anions adsorbed, meaning that the total number of in-pore ions does not change significantly. For the 0.5 M electrolyte, an apparent increase in in-pore cation population is observed between 1.0 → 1.5 V. However, for these voltages we note there are larger uncertainties in deconvoluting the very low intensity in-pore resonances in the experimental ^{31}P NMR spectra. In the negative voltage range, a different charging mechanism is observed: between 0 → –1.5 V, the in-pore cation population increases for all electrolyte concentrations, but there are no significant changes in the in-pore anion population. Therefore charge storage in the negative voltage range is dominated by counter-ion adsorption, with an overall increase in the number of in-pore ions. Note that while the electrochemical stability

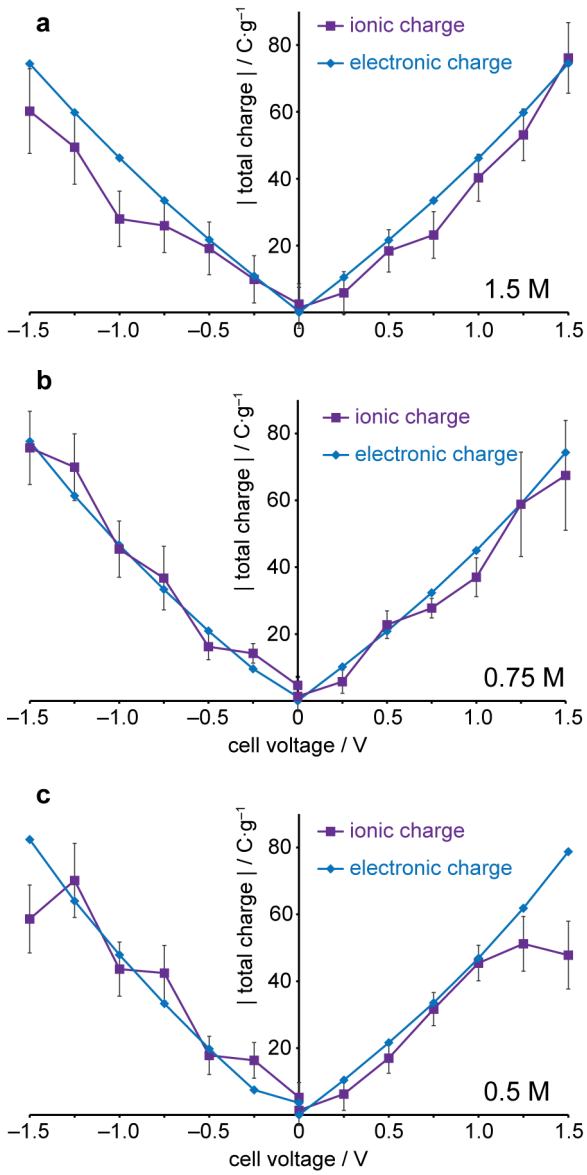

Figure 5. Comparisons of the magnitudes of ionic and electronic charge stored on supercapacitor electrodes in the range –1.5 – 1.5 V for electrolyte concentrations of (a) 1.5 M, (b) 0.75 M and (c) 0.5 M. Values are given as coulombs per gram of YP-50F carbon in a single electrode. Lines joining the data points are a guide to the eye. Good overall agreement between the stored electronic charge and ionic charge is observed across the voltage range studied.

window of ACN-based electrolytes can be as large as 3 V, the potential range studied here was limited to ±1.5 V due to the significant overlap of the in-pore and ex-pore resonances at > 1.5 V.

It is straightforward to determine the total ionic charge within the carbon electrode at each voltage step from the in-pore ion populations. For the three concentrations studied, we find good overall agreement between the ionic charge inside the micropores and the stored electronic charge (Fig. 5), the latter being determined from integration of the current vs time plots at each voltage step. At high voltages between 1 and 1.5 V for the 0.5 M electrolyte, a noticeable deviation is observed; this is likely related to the difficulty in accurately deconvoluting the weak ^{31}P in-pore resonance intensity at these voltages, the signal overlapping with the stronger signal from the ex-pore ions. The overall agreement between the ionic and electronic charge shows that it is the ions in the in-pore environment (within a few nanometres from the electrode surface) that are primarily responsible for charge storage.

To probe the local environments of the solvent molecules, *in situ* ^{2}H NMR spectra were recorded for a supercapacitor cell containing 1.5 M electrolyte (see Supplementary Information). The resonances corresponding to in-pore and ex-pore / free electrolyte ACN solvent molecules are much broader, probably as a result of faster exchange processes affecting the highly mobile solvent molecules, precluding the accurate deconvolution of in-pore resonance intensities. Instead, to gain further information about the charging mechanisms and behaviour of the solvent molecules, the same system was studied *in situ* using an electrochemical quartz crystal microbalance (EQCM). Particles of YP-50F carbon were deposited on a piezoelectric quartz crystal resonator whose resonance frequency can be related to the mass of the crystal electrode through the Sauerbrey equation,[27] thus providing information about the ion and solvent molecule fluxes during the charging of the porous carbon electrode. The carbon-coated resonator was used as a working electrode in a three-electrode EQCM cell containing PEt_4-BF_4 / ACN electrolyte at the intermediate concentration of 0.75 M. In contrast to previous EQCM studies, which probed dynamic charging using cyclic voltammetry experiments,[14,15] measurements were performed under steady-state conditions (*i.e.*, at fixed voltages) to mirror the NMR experimental methodology. These steady-state experiments should be less influenced by the kinetics of adsorption; rather, a complete reorganization of the ions and solvent molecules in the pores to approach the lowest energy arrangements is possible.

The electrode was polarised from the open-circuit voltage (OCV) of 0.43 V vs. Ag reference electrode up to +0.7 V vs. Ag in steps of 0.1 V. The electrode was then discharged to the OCV before being charged to 0 V vs. Ag in steps of –0.1 V. The electrode was held at each voltage for 120 s until a constant residual current was obtained (Fig. S9 in Supplementary Information). The initial OCV was close to the point of zero charge (PZC) of the electrode (0.49 V vs. Ag), the PZC being measured in a separate experiment (see Supplementary Information). The sequence was repeated several times to ensure reproducibility of the results. The low carbon loading on the resonator (tens of micrograms) restricts the electrochemical window such that purely capacitive behaviour is only observed in the potential range 0 ↔ +0.7 V vs. Ag. Outside of this window, there are significant redox contributions to the total current (see Fig. S10 in Supplementary Information).

Measured mass changes (normalized by the electrochemically active area of the quartz resonator, 1.27 cm^2) are plotted as a function of the electrode potential in Fig. 6a. The mass of the electrode is observed to increase at negative potentials relative to the OCV. This behaviour is qualitatively consistent with the adsorption-driven charging mechanism inferred from the NMR data, the absorption of cations into the micropores with no significant change in the anion

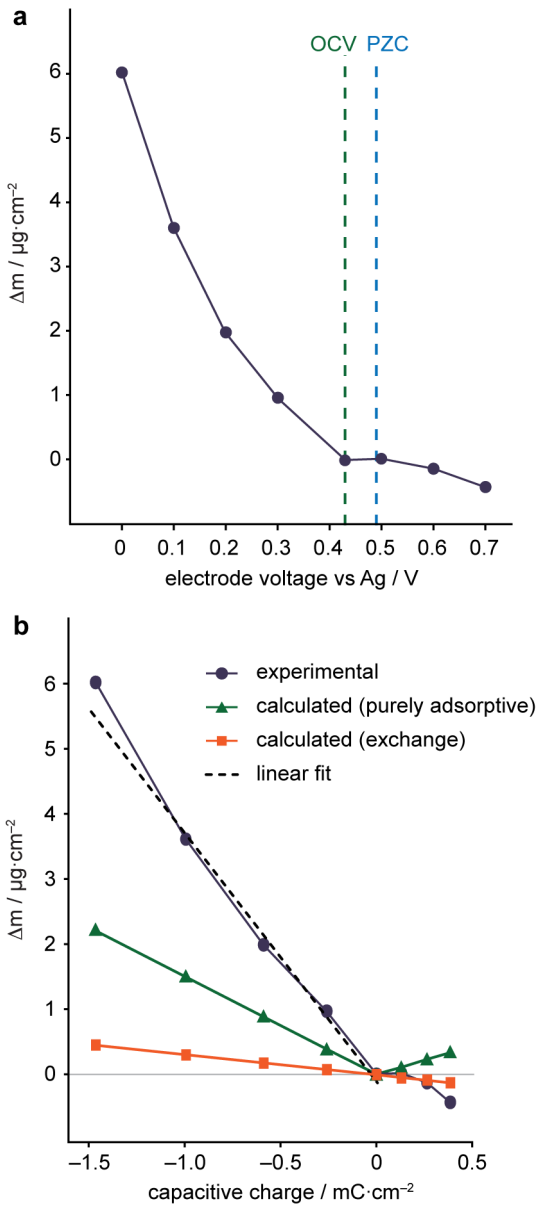

Figure 6. (a) Electrode mass change, Δm, plotted as a function of potential during polarization of YP-50F in 0.75 M PEt_4-BF_4 / ACN solution. The vertical dashed line denotes the open circuit potential (OCV). A mass increase is measured for negative polarization, whereas a mass decrease is measured for positive polarization (b) Comparison of experimental and calculated electrode mass changes plotted as a function of capacitive charge during polarization. Calculated mass changes are based on a purely adsorptive mechanism (green triangles) and an ion exchange mechanism (orange squares). The grey horizontal line denotes zero mass change. For negative polarization, a linear fit to the data (dotted line) shows experimental mass changes are larger than predicted by the purely adsorptive model, indicating that solvent molecules are also adsorbed. For positive polarization, the ion exchange mechanism gives best agreement with negative mass change observed experimentally.

population resulting in an increase in the total number of ions and hence mass of the electrode. For positive potentials relative to OCV, the electrode mass is found to decrease slightly over the potential range studied. This behaviour is consistent with the exchange-driven charging mechanism determined from the NMR data. The adsorption of anions and simultaneous explusion of cations from the electrode should result in an overall decrease in the total in-pore ionic mass since the BF_4 anions have a significantly smaller mass (86.8 g·mol^{-1}) than the PEt_4 cations (147 g·mol^{-1}).

It is possible to gain a more quantitative interpretation of the EQCM results by comparing the experimental mass changes with theoretical values calculated assuming different models for

the charging mechanism. Fig. 6b shows the experimental mass changes plotted as a function of the capacitive charge stored on the electrode, calculated by integrating current vs. time plots using Faraday's law.[15] Also plotted are theoretical mass changes based on two different charging mechanisms. For the first model, a purely adsorptive mechanism is considered, based on the traditional assumption that that one negative (positive) charge stored in the electrode is balanced by the adsorption of a single cation (anion) on the electrode surface. For the second model, an ion exchange mechanism was assumed whereby for positive (negative) electrode polarization, two charges stored on the electrode surface are compensated by the adsorption of one anion (cation) and desorption of one cation (anion). For negative polarization, the purely adsorptive model (green triangles) predicts the largest mass change, although the measured mass changes are much higher than those predicted by either model across the entire potential range. In contrast to the NMR data shown in Fig. 3, which selectively observe in-pore cation and anion populations, mass changes measured by EQCM originate from all electrolyte species (including solvent molecules) that enter and leave the porous electrode. Since the NMR data shows that the anion population remains approximately constant during negative polarization (*i.e.*, a purely adsorptive mechanism is operating), the additional mass observed experimentally must originate from the co-absorbed solvent molecules. The slope of a linear fit of the experimental mass change vs. charge gives an experimental molar mass of 369 $g \cdot mol^{-1}$ per adsorbed species (from Faraday's law). Assuming that the adsorbed species are PEt_4 cations (justified on the basis of the NMR results), we can estimate a cation solvation number of 5.4. This value is slightly lower than the solvation number of 7 predicted for chemically similar NEt_4 cations in bulk solution,[26] indicating that cations are partially desolvated when they enter the pores of the microporous carbon.

For positive polarization, Fig. 6b shows that the purely adsorptive model again predicts a mass increase as BF_4 anions are absorbed into the micropores. This is not in agreement with the experimental data, where a slight mass decrease is observed. In contrast, the ion exchange model (orange squares) predicts a slight decrease in electrode mass during charging. This is because heavier PEt_4 cations (147.2 $g \cdot mol^{-1}$) are replaced by an equal number of lighter BF_4 anions (86.8 $g \cdot mol^{-1}$) in the electrode. This model gives better agreement with the experimental values, where a mass decrease is also observed. Although it was not possible to extract clear information regarding the solvation number because of the limited accessible voltage window at positive potentials (up to 0.7 V vs. Ag) and low deposited mass of carbon, the fact that change of the electrode mass follows that predicted by the NMR results confirms that the charging mechanism is driven by ion exchange in the potential range studied. For the 0.75 M and 0.5 M electrolyte concentrations, a large fraction of the cations are expelled at the highest potential studied by NMR (+1.5 V, see Figures 4b and c). As a consequence, the purely adsorptive mechanism must start to

become important at higher potential when all cations have been expelled from the electrode. However, the restricted potential range of the EQCM measurements (from 0 to 0.7 V vs Ag) prevents high polarisation states to be reached. We note that in this regime (> 1.5 V), the EQCM response of the electrode would be expected to change to show increasing mass for the positive electrode (reflecting a purely adsorptive mechanism).

Discussion

The combined NMR-EQCM approach provides a full picture of the charge storage mechanism over the potential range studied. At a cell voltage of 0 V, the electrode is wetted by equal numbers of anions and cations, which are densely packed inside the micropores and partially desolvated for high electrolyte concentrations. Upon charging, for negative potentials the electronic charge stored on the electrode surface is balanced by the absorption of cations into the micropores. For positive potentials, the stored electronic charge is balanced by the absorption of anions into the micropores and simultaneous expulsion of cations.

The asymmetry in ion sizes may be one reason for the different mechanisms in the two charging regimes. Ion and solvent reorganization inside the micropores may play a role in determining this: packing inside of the pores may be more efficient with excess (spherical) cations than for excess anions, so that more charge can be accommodated at negative potentials without having to expel the co ions. Of note, the EQCM measurements for the current system indicate that the adsorbed cations also carry additional solvent molecules into the pores, which means that even more space has to found inside the micropores as the electrode is charged. Under the steady-state conditions employed here, and in contrast to dynamic measurements performed in other EQCM studies, solvent molecules will have time to reorder so that they can take up less space. We note that the ordering of propylene carbonate (PC) solvent molecules within micropores has recently been observed by X-ray total scattering experiments.[28] Pair distribution function analysis identified a shortening of the average intermolecular distance by approximately 0.05 Å as compared to bulk solution, interpreted as a densification of the packing of the PC molecules through vertical alignment. It is also possible that the micropores may expand during charging to accommodate the additional adsorbed species. Indeed, the expansion of micropores during charging has recently been proposed on the basis of electrochemical dilatometry experiments.[29] The results presented here should be contrasted with our earlier work on a 1.5 M tetraethylammonium tetrafluoroborate (NEt_4-BF_4) / ACN electrolyte.[22] In this work, only the anions were monitored by ^{19}F NMR; for negative potentials the in-pore anion population changed only slightly upon charging to –0.5 V (as seen here), after which it dropped to approximately 20% of the initial value at –1.25 V. At positive potentials, the in-pore anion population remained constant

until approximately 0.75 V before increasing steadily. Although we can only indirectly infer NEt_4 cation behaviour, these results suggest that charge is stored via the cation adsorption mechanism now in a different potential window (–0.5 to +0.75 V (NEt_4^+) vs. –1.5 to 0.0 V (PEt_4^+)). It is possible that the screening between cations may be worse for the smaller, less polarisable NEt_4 cations, disfavouring dense cation packing, and reducing the negative voltage threshold at which anions are expelled from the pores. Differential solvation effects for the two types of cation may also be important.

Kinetic phenomena cannot be totally excluded. Unlike the current study which was performed on a pristine cell, the cells in the previous study[22] were cycled multiple times between 0 – 2.3 V prior to the NMR measurements. Furthermore, magnetic resonance imaging experiments, albeit under non-steady state conditions, have indicated that changes in in-pore ion populations can occur in the first several cycles;[24] this will further affect ion transport and ordering in the electrode during charging. In the current study, the adsorption of larger cations at negative polarizations could present steric hindrance to anions leaving the pores. However, the steady-state conditions employed in this work, and the rapid mobility of both the cations and anions, should allow ions and solvent molecules to reorganize within the pores (and within the electrolyte) to approach the lowest energy state. Hence, it is unlikely that kinetic effects are dominant in determining the in-pore ionic populations at different charge states, unless the differences in energy between the ion-exchange vs. ion adsorption are very small. Experiments are underway to study an even wider range of systems under both static and dynamic charging conditions to explore these phenomena further.

The experiments provide definitive evidence that over most potential ranges the electric double layer formed during charging is *not* composed of a single counter-ionic species, the NMR results showing that significant numbers of co-ions can remain inside the micropores during charging in both the positive and negative voltages ranges. However, for the positive electrode in the 0.5 M concentration electrolyte the cations are almost completely ejected from the electrode at a cell voltage of around 1 V while anions continue to be adsorbed. Mean field theory and simulations have shown that for certain pore/ion size ratios, a ‘jump’ in capacitance can be expected for such a case, *i.e.*, where the applied potential is sufficiently high to drive the co-ions out of the pore but is not high enough to fill the pores completely with counter-ions.[10,30] No significant capacitance increase was measured for the 0.5 M concentration electrolyte as compared to the 1.5 M electrolyte (both yielding capacitances of approximately 100 $F \cdot g^{-1}$ (see Supplementary Information)); however, it may be that factors such as charge screening by solvent molecules or the appreciable pore-size distribution of YP-50F mask any effects in this case. Future

investigations will enable a better fundamental understanding of the relative importance of these effects for the optimization of capacitive properties.

In conclusion, we have used *in situ* NMR spectroscopy to quantify fully the cationic and anionic species within the electric double-layer in a working supercapacitor electrode. The combination of *in situ* NMR and EQCM measurements also gives further information on solvent uptake during charging that is not possible using either technique alone. Our results provide a direct molecular-level insight into the charge storage process in microporous carbon electrodes, and show that the charging mechanisms differ depending on the polarization of the electrode surface. The methodology introduced here opens the way for the study of factors such as relative pore/ion sizes, concentration and solvent effects on the ionic composition of the electric double-layer during charging, questions that are at the heart of current efforts to optimize and improve the energy storage capabilities of supercapacitors.

Materials and Methods

All carbon electrodes were prepared from YP-50F activated carbon (Kuraray Chemical, Japan). Free-standing carbon films were prepared as reported in Ref. 23 by mixing carbon powder (95 wt %) with polytetrafluoroethylene (5 wt %) (Sigma Aldrich, 60 wt % dispersion in water). Films were rolled to an approximate thickness of 0.25 mm. Prior to sample preparation, carbon film pieces were dried under vacuum at 200 °C overnight and then transferred to an argon glove box with H_2O and O_2 levels less than 0.1 ppm. Inside the glove box, the film pieces were cut to a mass of 7.4 ± 0.1 mg. Tetraethylphosphonium tetrafluoroborate salt (>98%) was obtained from Tokyo Chemical Industries. Supercapacitor bag cells were prepared as previously described.[22] NMR experiments were performed using a Bruker Avance spectrometer operating at a magnetic field strength of 7.05 T, corresponding to ^{19}F and ^{31}P Larmor frequencies of 284.2 and 121.5 MHz, respectively. A Bruker HX double resonance static probe was used, with a 6.8 mm inner diameter solenoid coil. ^{19}F NMR spectra are referenced relative to neat hexafluorobenzene (C_6F_6) at −164.9 ppm, and ^{31}P NMR spectra are referenced relative to 85 wt% $H_3PO_{4(aq)}$ at 0 ppm. More details on the *in situ* methodology and deconvolution of the NMR spectra are given in Supplementary Information.

For EQCM measurements, a slurry composed of 80-90% of active electrode materials and 10-20% of polyvinylidene fluoride (Arkema) in *N*-methyl-2-pyrrolidone (Sigma-Aldrich) was prepared and few droplets were deposited on a Maxtek 1 inch-diameter Au-coated quartz crystal resonator (with a fundamental frequency of 5 MHz). The carbon-coated quartz resonator was then dried at 60°C overnight in air. Maxtek RQCM system was combined with an Autolab PGSTAT101 potentiostat for simultaneous EQCM and electrochemical measurements. Details of the cell assembly were reported previously.[15] Chronoamperometry tests were conducted at room temperature with simultaneous recording of the quartz resonance frequency. The capacitive charge stored on the electrode was calculated by integrating the current versus step duration time during the potential hold (see Fig. S9). Further details are given in Supplementary Information.

Acknowledgements

ACF, JMG and CPG acknowledge the Sims Scholarship (ACF), EPSRC (via the Supergen consortium for JMG) and the EU ERC (via an Advanced Fellowship to CPG) for funding. PS and WYT acknowledge support from the European Research Council (ERC, Advanced Grant, ERC-2011-AdG, Project 291543 – IONACES). P.S. also acknowledges funding from the Chair "Embedded Multi-Functional Nanomaterials" from the Airbus Group Foundation. ACF and JMG thank the NanoDTC Cambridge for travel funding. We also thank Alexei Kornyshev, Svyatoslav Kondrat and Céline Merlet for useful discussions.

Author contributions

JMG, ACF and CPG designed the research. JMG made supercapacitor cells and electrolytes, performed NMR experiments and analysed the NMR data. W-YT, PLT and PS designed the EQCM work. W-YT carried out the EQCM experiments and W-YT, PLT and PS analysed the data. All authors contributed to discussion of the data and writing the paper.

Competing financial interests

The authors declare no competing financial interests.

References

1. Salitra, G., Soffer, A., Eliad, L., Cohen, Y. & Aurbach, D. Carbon electrodes for double layer capacitors. I. Relations between ion and pore dimensions. *J. Electrochem. Soc.*, **147**, 2486-2493 (2000).

2. Chmiola, J., Yushin, G., Gogotsi, Y., Portet, C., Simon, P. & Taberna, P.-L. Anomalous increase in carbon capacitance at pore sizes less than 1 nanometer. *Science*, **313**, 1760-1763 (2006).

3. Largeot, C., Portet, C., Chmiola, J., Taberna, P.-L., Gogotsi, Y. & Simon, P. Relation between the ion size and pore size for an electric double-layer capacitor. *J. Am. Chem. Soc.*, **130**, 2730-2731 (2008).

4. Vix-Guterl, C., Fracowiak, E., Jurewicz, K., Friebe, M., Parmentier, J. & Beguin, F. Electrochemical energy storage in ordered porous carbon materials. *Carbon*, **43**, 1293-1302 (2005).

5. Chmiola, J., Largeot, C., Taberna, P.-L., Simon, P & Gogotsi, Y Desolvation of ions in subnanometer pores and its effect on capacitance and double-layer theory. *Angew. Chem. –Int. Ed.*, **47**, 3392-3395 (2008).

6. Fedorov, M. V. & Kornyshev, A. A. Ionic liquids at electrified interfaces. *Chem. Rev.*, **114**, 2978-3036 (2014).

7. Burt, R., Birkett, G. & Zhao, X. S. A review of molecular modeling of electric double layer capacitors. *Phys. Chem. Chem. Phys.*, **16**, 6519-6538 (2014).

8. Feng, G. & Cummings, P. T. Supercapacitor capacitance exhibits oscillatory behaviour as a function of nanopore size. *J. Phys. Chem. Lett.* **2**, 2859-2864 (2011).

9. Wu, P., Huang, J., Meunier, V., Sumpter, B. G. & Qiao, R. Complex capacitance scaling in ionic liquids-filled nanopores. ACS Nano, **5**, 9044-9051 (2011).

10. Kondrat, S. & Kornyshev, A. Superionic state in double-layer capacitors with nanoporous electrodes. *J. Phys.: Condens. Matter*, **23**, 022201 (2011).

11. Merlet, C., Rotenbeg, B., Madden, P. A., Taberna, P.-L., Simon, P., Gogotsi, Y. & Salanne, M. On the molecular origin of supercapacitance in nanoporous carbon electrodes. *Nature Mater.* **11**, 306-310 (2012).

12. Merlet, C., Péan, C, Rotenburg, B., Madden, P. A., Daffos, B., Taberna, P.-L., Simon, P & Salanne, M. Highly confined ions store charge more efficiently in supercapacitors. *Nature Commun.*, **4**, 2701 (2013).

13. Kondrat, S., Wu, P., Qiao, R. & Kornyshev, A. A. Accelerating charging dynamics in subnanometre pores. *Nature Mater.,* **13**, 387-393 (2014).

14. Levi, M. D, Salitra, G., Levy, N., Aurbach, D. & Maier J. Application of a quartz-crystal microbalance to measure ionic fluxes in microporous carbons for energy storage. *Nature Mater.* **8**, 872-875 (2009).

15. Tsai, W.-Y., Taberna, P.-L. & Simon, P. Electrochemical quartz crystal microbalance (EQCM) study of ion dynamics in nanoporous carbons. *J. Am. Chem. Soc.*, **136**, 8722-8728 (2014).

16. Richey, F. W., Dyatkin, B., Gogotsi, Y., Elabd, Y. A. Ion dynamics in porous carbon electrodes in supercapacitors using in situ infrared spectroelectrochemistry. *J. Am. Chem. Soc.*, **135**, 12818-12826 (2013).

17. Richey, F. W., Tran, C., Kalra, V. & Elabd, Y. A. Ionic liquid dynamics in nanoporous carbon nanofibers in supercapacitors measured with in operando infrared spectroelectrochemistry. *J. Phys. Chem. C*, **118**, 21846-21855 (2014).

18. Forse, A. C., Griffin, J. M., wang, H., Trease, N. M., Presser, V., Gogotsi, Y., Simon, P. & Grey, C. P. Nuclear magnetic resonance study of ion adsorption on microporous carbide-derived carbon. *Phys. Chem. Chem. Phys.*, **15**, 7722-7730 (2013).

19. Borchardt, L., Oschatz, M., Paasch, S., Kaskel, S. & Brunner, E. Interaction of electrolyte molecules with carbon materials of well-defined porosity: characterization by solid-state NMR spectroscopy. *Phys. Chem. Chem. Phys.*, **15**, 15177-15184 (2013).

20. Deschamps, M., Gilbert, E., Azais, P., Raymundo-Piñero, E., Ammar, M., R., Simon, P., Massiot, D. & Beguin, F. Exploring electrolyte organization in supercapacitor electrodes with solid-state NMR. *Nature Mater.*, **12**, 351-358 (2013).

21. Wang, H., Köster, T. K.-J., Trease, N. M., Ségalini, J., Taberna, P.-L., Simon, P., Gogotsi, Y. & Grey C. P. Real-time NMR studies of electrochemical double-layer capacitors. *J. Am. Chem. Soc.*, **133**, 19720-19273 (2011).

22. Wang, H., Forse, A. C., Griffin, J. M., Trease, N. M., Trognko, L., Taberna, P.-L., Simon, P. & Grey, C. P. In situ NMR spectroscopy of supercapacitors: insight into the charge storage mechanism. *J. Am. Chem. Soc.*, **135**, 18968-18980 (2013).

23. Griffin, J. M., Forse, A. C., Wang, H., Trease, N. M., Taberna, P.-L., Simon, P. & Grey, C. P. Ion counting in supercapacitor electrodes using NMR spectroscopy. *Faraday Discuss.,* (2014) *Accepted for publication.*

24. Ilott, A. J., Trease, N. M., Grey, C. P. & Jerschow, A. Multinuclear in situ magnetic resonance imaging o electrochemical double-layer capacitors. *Nature Commun.* **5**, 4536 (2014).

25. Forse, A. C., Griffin, J. M., Presser, V., Gogotsi, Y & Grey C. P. Ring current effects: factors affecting the NMR chemical shift of molecules adsorbed on porous carbons. *J. Phys. Chem. C*, **118**, 7508-7514 (2014).

26. Kim, Y.-J., Masutzawa, Y., Ozaki, S., Endo, M. & Dresselhaus, M. S. PVDC-based carbon material by chemical activation and its application to nonaqueous EDLC. *J. Electrochem. Soc.*, **151**, E199-E205 (2004).

27. Sauerbrey, G. Verwendung von Schwingquarzen zur Wägung dünner Schichten und zur Mikrowägung [The use of resonance quartz crystals for weighing thin layers and as a microbalance] *Z. Für Phys.* **155**, 206-222 (1959).

28. Fukano, M., Fujimori, T., Ségalini, J., Iwama, E., Taberna, P.-L., Iiyama, T., Ohba, T., Kanoh, H., Gogotsi, Y., Simon, P. & Kaneko, K. Vertically oriented propylene carbonate molecules and tetraethyl ammonium ions in carbon slit pores. *J. Phys. Chem. C*, **117**, 5752-5757 (2013).

29. Hantel, M. M., Presser, V., Kötz, R. & Gogotsi, Y. In situ electrochemical dilatometry of carbide-derived carbons. *Electrochem. Commun.*, **13**, 1221-1224 (2011).

30. Kondrat, S., Georgi, N., Fedorov, M. V., & Kornyshev, A. A. A superionic state in nano-porous double-layer capacitors: Insights from Monte Carlo simulations. *Phys. Chem. Chem. Phys.*, **13**, 11359-11366 (2011).

In Situ NMR and Electrochemical Quartz Crystal Microbalance Measurements Reveal the Structure of the Electric Double-Layer in Supercapacitor Electrodes

John M. Griffin, Alexander C. Forse,

Wan-Yu Tsai, Pierre-Louis Taberna, Patrice Simon, and Clare P. Grey

Supplementary Information

1. Quantifying adsorbed species at zero applied potential

2. Estimated Solvated Ion Diameters

3. *In situ* NMR spectra of solvent molecules

4. Additional NMR details

5. *In Situ* NMR Methodology

6. Electrochemical characterisation of *in situ* NMR supercapacitor bag cells

7. NMR spectra of dried supercapacitor electrodes

8. Electrochemical quartz crystal microbalance experiments

9. Gas sorption experiments on YP-50F

1. Quantifying adsorbed species at zero applied potential

To quantify adsorbed species at zero applied potential, a series of calibration bag cells were prepared, each containing a 7.4 ± 0.1 mg YP-50F film electrode soaked with accurately measured volumes of electrolyte between 2 and 12 µL. ^{31}P and ^{19}F NMR spectra of bag cell samples with 1.5 M electrolyte concentration are shown in Figure S1.

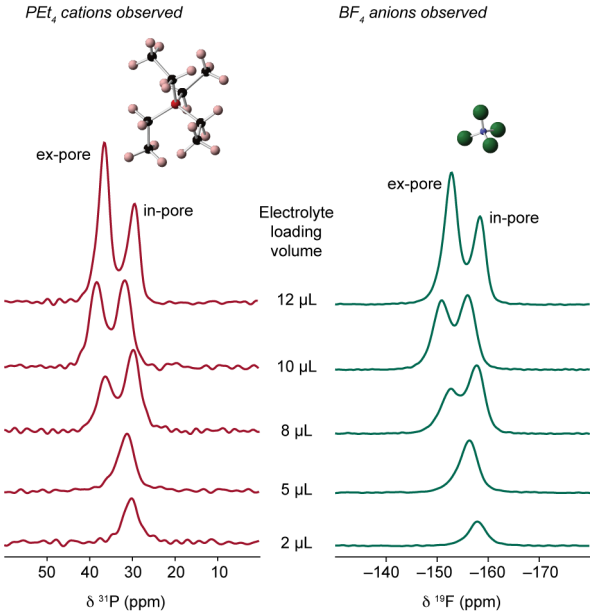

Figure S1. ^{31}P and ^{19}F NMR spectra of bag cells containing 7.4 ± 0.1 mg YP-50F films soaked with different volumes of 1.5 M PEt_4-BF_4 / ACN electrolyte.

The NMR spectra of the calibration bag cell samples were fitted with two resonances (corresponding to in-pore and ex-pore environments), and linear fits were performed for the total intensity as a function of electrolyte volume. Since the electrolyte concentrations and total sample volumes are known, it is then possible to quantify the absolute number of ions for a given resonance intensity in the NMR spectrum.

However, accurate comparisons between the resonance intensities of the calibration samples and the resonance intensities determined for the supercapacitor cells are not possible because the metal current collectors have a large effect on the radiofrequency properties of the NMR probe, resulting in significant changes to the pulse lengths and powers, and detected signal amplitudes. Instead, 'dummy' supercapacitor cells were constructed, containing two electrodes separated by a small reservoir of electrolyte (as shown in Figure S2). In-pore resonance intensities for the dummy cell electrodes can be directly compared with the calibration samples because they do not contain metal components. Furthermore, these cells contain electrodes in the same environment as in a supercapacitor device, *i.e.*, fully saturated with electrolyte.

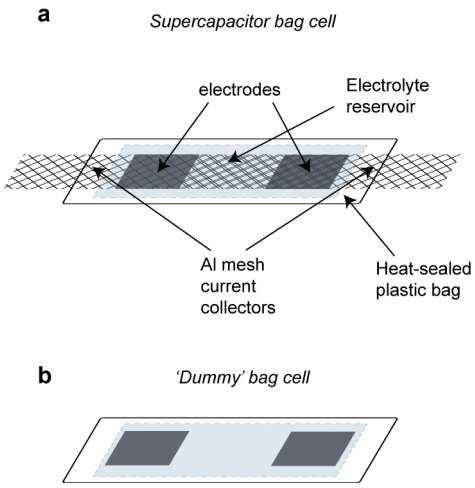

Figure S2. Schematic diagram showing the construction of (a) an 'overlaid' design supercapacitor bag cell, and (b) a dummy cell without current collectors for calibration experiments.

This dummy cells enable the determination of the number of in-pore ions in a 7.4 ± 0.1 mg electrode which is saturated in electrolyte with no applied potential. Since the working supercapacitor cells contained electrodes of the same mass, the same number of in-pore ions was assumed at 0 V.

2. Estimated Solvated Ion Diameters

The solvated BF_4 anion diameter of 1.16 nm is based on the value determined using the Cerius 3.8 program in Ref. [S1]. This assumes a single solvation shell comprising 9 acetonitrile molecules.

For the PEt_4 cation, no literature data for the solvated ion diameter is available. However, a recent publication by Matsumoto *et al*. provides crystallographic data for PEt_4-BF_4 salt, giving a desolvated cation diameter of approximately 0.72 nm.[S2] Assuming the thickness of the solvation shell to be the same as that for the tetraethylammonium (NEt_4) cation (calculated in Ref [S1]. to be 0.32 nm for a solvation shell comprising 7 acetonitrile molecules), we may estimate the solvated PEt_4 cation diameter to be 1.35 nm.

3. *In situ* NMR spectra of solvent molecules

To probe the local environments of the solvent molecules, ^2H NMR spectra were recorded for a supercapacitor cell containing 1.5 M PEt_4-BF_4 / ACN with deuterated solvent. As shown in Figure S3a, at 0 V, resonances corresponding to in-pore and ex-pore / free electrolyte ACN solvent molecules are observed, although in this case the linewidths are much broader; this is likely to be a result of faster exchange processes affecting the highly mobile solvent molecules and possibly residual ^2H quadrupolar interactions. While the broader resonances preclude an accurate deconvolution of the in-pore resonance intensities, qualitative differences in the behaviour of the

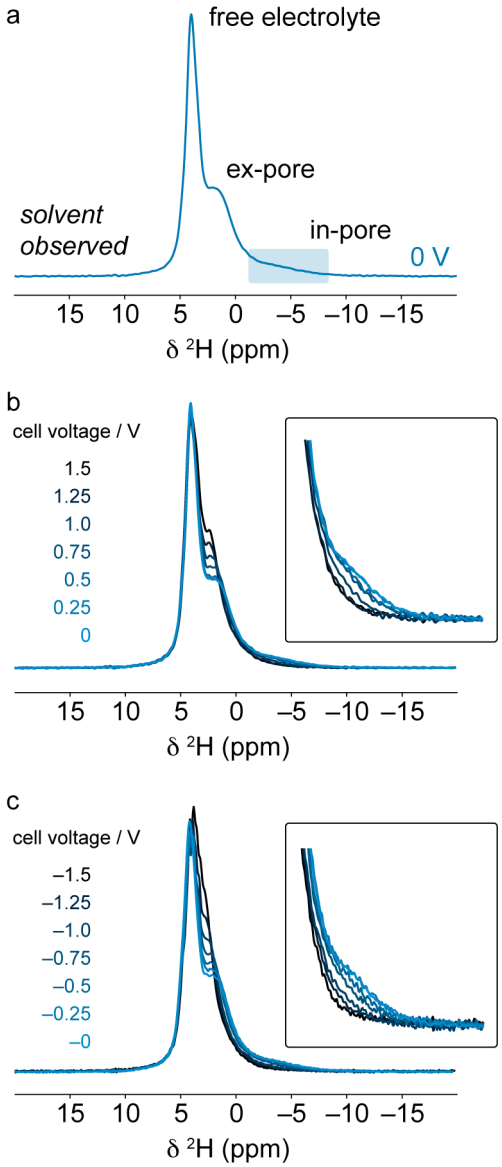

Figure S3. (a) ^{2}H NMR spectrum of a supercapacitor cell containing 1.5 M PEt_4-BF_4 / ACN electrolyte with deuterated solvent. In-pore, ex-pore and free electrolyte solvent environments are observed. (b, c) *In situ* ^{2}H NMR spectra recorded as the capacitor is charged between –1.5 and +1.5 V.

in-pore resonances are observed in the two charging regimes. In the positive charging regime (Figure S3b), the in-pore resonance is observed to move to high frequency underneath the ex-pore / free electrolyte feature as the supercapacitor is charged, as is observed in the NMR spectra of the electrolyte ions. The intensity of the ex-pore feature increases as the in-pore feature moves underneath it. For the negative charging regime (Figure S3c), the movement of the resonance to high frequency appears to be accompanied by a larger increase in the intensity of the ex-pore feature. This could indicate that the in-pore solvent molecule population increases during negative charging, which is consistent with the EQCM data showing that the adsorbed cations are partially solvated.

4. Additional NMR details

NMR experiments were performed using a Bruker Avance spectrometer operating at a magnetic field strength of 7.05 T, corresponding to ^{19}F and ^{31}P Larmor frequencies of 284.2 and 121.5 MHz, respectively. A Bruker HX double-resonance static probe was used, with a 6.8 mm inner diameter solenoid coil. The "depth" pulse sequence[S3] was used for all experiments in order to reduce the background and probe ringing signals. The total delay between excitation of transverse magnetization and acquisition of the free induction decay was 90 μs. A recycle interval of 30 s was used, which was sufficient for spectra to be quantitative. For ^{19}F NMR experiments, 16 transients were coadded for each spectrum; for ^{31}P NMR experiments, 128 (256) transients were coadded for spectra recorded for samples containing 1.5 M (0.75 M & 0.5 M) electrolyte. ^{19}F NMR spectra are referenced relative to neat hexafluorobenzene (C_6F_6) at −164.9 ppm, and ^{31}P NMR spectra are referenced relative to 85 wt% $H_3PO_{4(aq)}$ at 0 ppm.

5. *In Situ* NMR Methodology

In situ NMR experiments were carried out by placing the pristine cell in the NMR coil in the vertical orientation[S4] and charging sequentially to a series of different voltages (0, 0.25, 0.5, 0.75, 1, 1.25, 1.5, 0, –0.25, –0.5, –0.75, –1, –1.25 and –1.5 V). The applied potential was controlled using a Bio-logic cycler in two-electrode configuration. Cells were held at each voltage for 60 minutes (1.5 M, 0.75 M electrolyte) or 90 minutes (0.5 M electrolyte) until an equilibrium charge state was obtained before ^{19}F and ^{31}P NMR spectra were acquired. For low voltages the current was close to zero at equilibrium. For voltages between 1 – 1.5 V, small constant currents of up to 0.005 mA were observed at equilibrium. For the discharge of the cell (1.5 → 0 V), current relaxations of double duration were used. Spectral fitting was carried out using DMfit software.[S5] Deconvolutions were carried out using a mixture of Gaussian and Lorentzian lineshapes to describe the different features in the spectra. In each case only the minimum number of components required to model the spectrum were used and a single lineshape was assumed for the in-pore resonance. Some spectra required several lineshapes to describe the free electrolyte / ex-pore resonance. This is ascribed to bulk magnetic susceptibility (BMS) effects and local variations in the magnetic field across the bag cell, which results in a range of different local fields and thus shifts for the same chemical species.[S5] For each electrolyte, the spectrum obtained at 0 V was fitted first, as this showed the best resolution of the in-pore resonance. The peak positions and intensities obtained were then used as a starting point to fit the spectrum at the next highest voltage. Fits were repeated up to four times for each series of data in order to estimate errors. Example deconvolutions of ^{31}P and ^{19}F NMR spectra are shown in Figure S4.

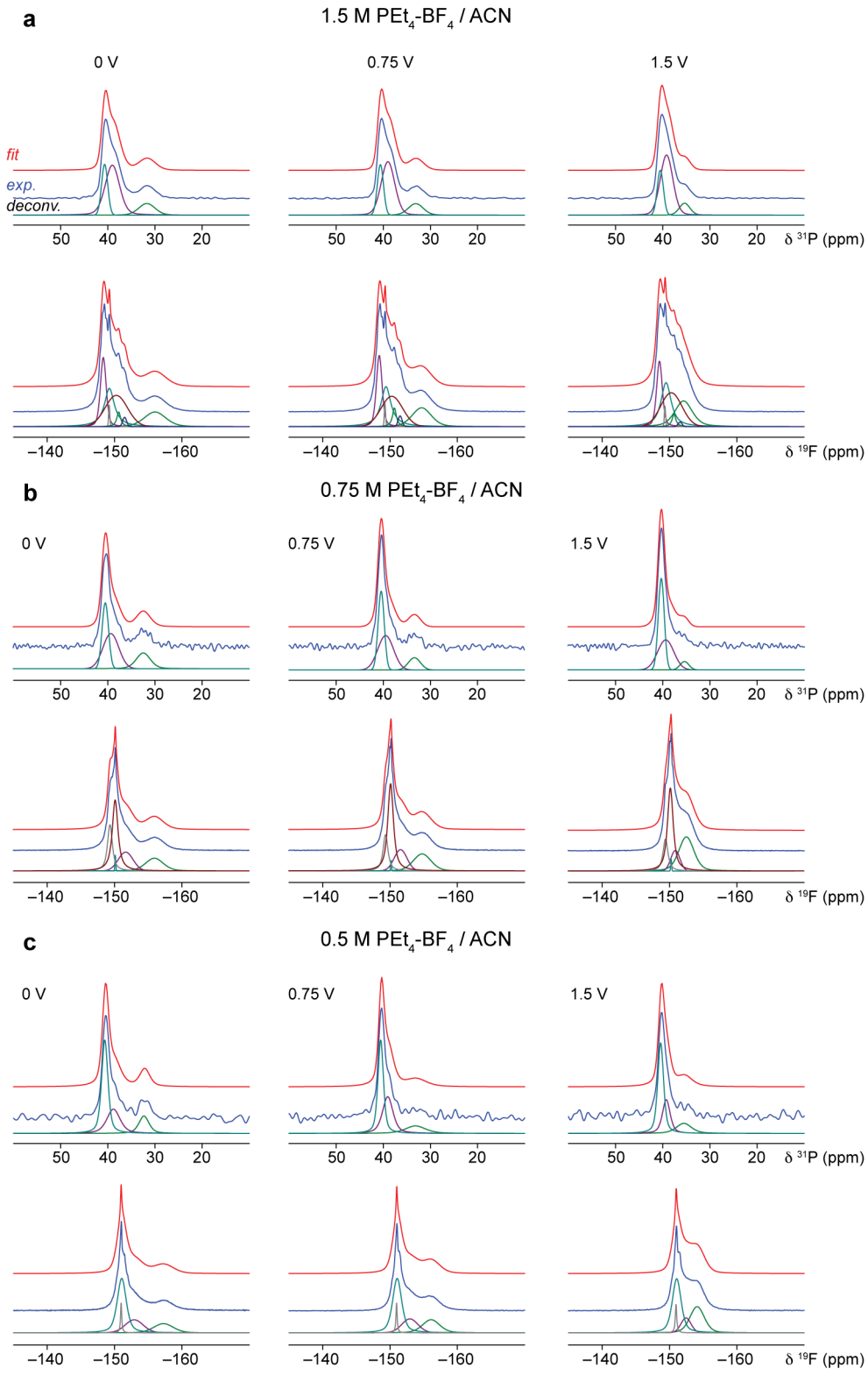

Figure S4. Representative deconvolutions of ^{31}P and ^{19}F *in situ* NMR spectra recorded for cells held at voltages of 0, 0.75 and 1.5 V. Experimental lineshapes are shown in blue, while the sum of individual fitted components is shown in red.

6. Electrochemical characterisation of *in situ* NMR supercapacitor bag cells

A cyclic voltammogram (CV) for a 1.5 M PEt_4-BF_4 / ACN supercapacitor bag cell with 7.4 mg YP-50F electrodes is shown in Figure S5. The CV was recorded between cell voltages of 0 and 1.5 V with a voltage scan rate of 0.5 $mV \cdot s^{-1}$. Reproducible capacitive behaviour was observed over 10 cycles, and the discharge current of –0.18 mA at 0.9 V yields a capacitance of 102.4 $F \cdot g^{-1}$. This is in good agreement with the capacitance obtained from the 1.5 V → 0 V discharge current in the *in situ* NMR experiment (see below), and values reported for similar systems in the literature.[S4,S6]

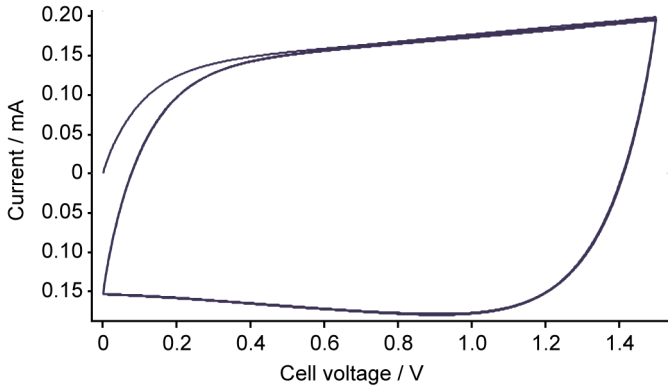

Figure S5. Cyclic voltammogram of 1.5 M PEt_4-BF_4 / ACN supercapacitor bag cell with 7.4 mg YP-50F electrodes.

Figure S6 shows current relaxations for the 1.5 M PEt_4-BF_4 / ACN supercapacitor bag cell with 7.4 mg YP-50F electrodes during the *in situ* NMR experiment. The relative timings and durations of the *in situ* NMR experiments are also shown. Small residual currents were obtained, with a maximum value of 1.8 μA at 1.5 V. These constant currents are attributed to non-faradaic processes and so are neglected in the calculation of total charge stored (Fig. 5 in the main text). Inclusion of these constant residual currents does not make a significant difference to the values obtained.

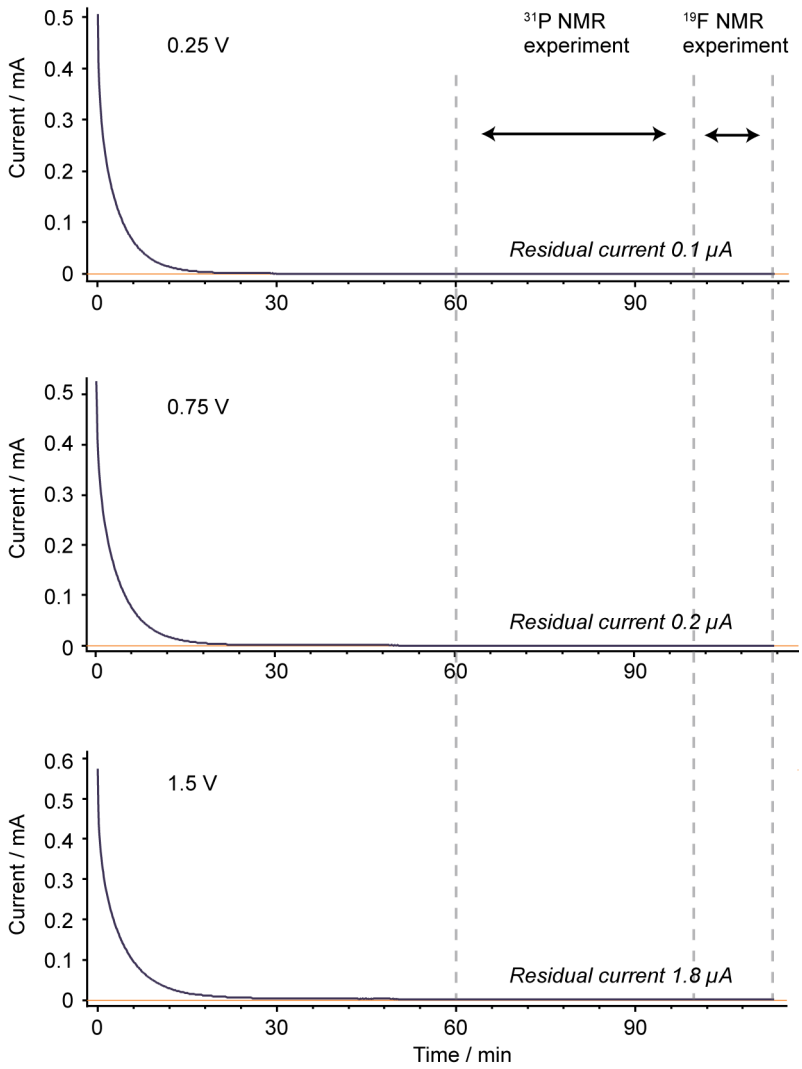

Figure S6. Current relaxations for the 1.5 M PEt_4-BF_4 / ACN supercapacitor bag cell with 7.4 mg YP-50F electrodes recorded during the *in situ* NMR experiment. Vertical dashed lines indicate the start and end points of ^{31}P and ^{19}F *in situ* NMR experiments performed sequentially after a constant current was obtained.

Figure S7 shows the cumulative charge stored for each cell at each voltage step in the *in situ* NMR experiments. The stored charge varies approximately linearly with the applied cell voltage in each case and is fully discharged during the 1.5 V → 0 V step.

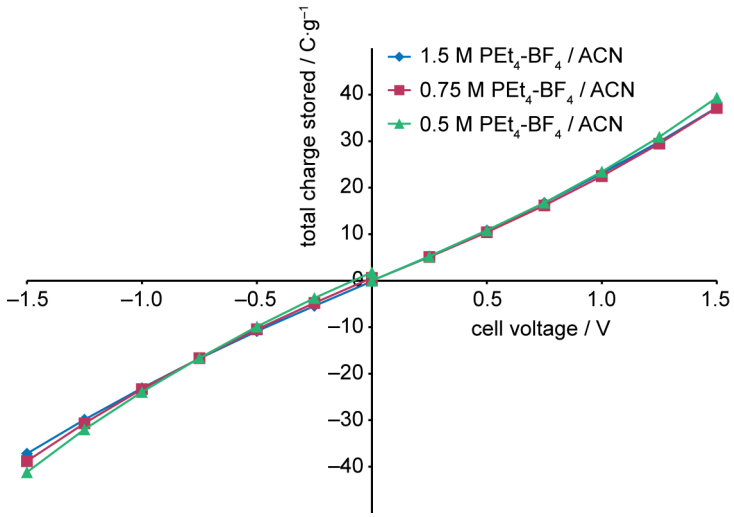

Figure S7. Plot showing cumulative charge stored as a function of voltage in supercapacitor bag cells containing 7.4 mg YP-50F electrodes used in *in situ* NMR experiments.

From integration of the 1.5 → 0 V discharge current with respect to time, a gravimetric capacitance of 99.6 $F \cdot g^{-1}$ was determined for the bag cell containing 1.5 M PEt_4-BF_4 / ACN electrolyte. This value is in good agreement with literature values for similar systems comprising activated carbon electrodes and tetraethylammonium tetrafluoroborate electrolyte.[S4,S6]

The capacitance of the cells containing 0.75 M and 0.5 M PEt_4-BF_4 / ACN electrolyte as determined from the integrated 1.5 → 0 V discharge currents were found to be 97.5 and 100.2 $F \cdot g^{-1}$, respectively, almost identical to the cell made with the 1.5 M electrolyte. This shows that, despite the differences in concentration, an essentially equal amount of charge is stored by these systems over the voltage range studied.

7. NMR spectra of dried supercapacitor electrodes

To investigate the effect of drying supercapacitor electrodes, 3.4 mg YP-50F carbon films were wetted with 5 µL of NEt_4-BF_4 / ACN and PEt_4-BF_4 / ACN electrolytes inside magic angle spinning NMR rotors. The rotors were then sealed before ^{19}F NMR spectra were recorded (shown in blue in Figure S8). Ex-pore and in-pore anion environments are clearly visible for both electrolytes. The NMR rotors were then opened and left in air for 45 minutes for the solvent to evaporate. ^{19}F NMR spectra of the dried films are shown in red in Figure S8. For both electrolytes, the evaporation of the solvent causes changes in the ex-pore ion populations (which decrease) and the in-pore anion populations (which increase). It is possible that as solvent molecules are removed from the ex-pore environment, the occupation of the in-pore environment becomes more energetically-favourable, where solvent molecules remain. These data show that differences in measured ion populations are to be expected between the *in situ* NMR experiments reported in this work, and *ex situ* experiments reported previously, where electrodes were dried prior to the NMR experiment.[S6]

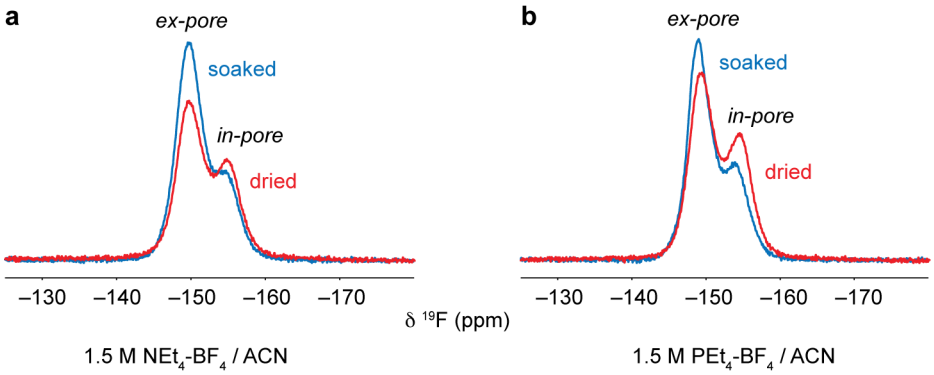

Figure S8. ^{19}F NMR spectra of YP-50F films wetted with 1.5 M (a) NEt_4-BF_4 / ACN and (b) PEt_4-BF_4 / ACN electrolyte (blue) and subsequently dried for 45 minutes in air (red). Clear changes in the ex-pore and in-pore ion populations are observed after drying.

8. Electrochemical quartz crystal microbalance experiments

YP-50F with 10-20% PVdF binder was drip-coated on a 5 MHz Maxtek 1-inch quartz crystal. Electrochemical measurements were conducted with simultaneous recording of the quartz resonance frequency (the details of cell assembly were reported previously[S7]).

The shift of the resonance frequency of the quartz resonator (Δf) can be converted into a mass change (Δm) of the quartz crystal and electrodes by applying Sauerbrey's equation (1):

$$\Delta m = -\frac{\sqrt{\rho_q \mu_q}}{2 f_o} \cdot \Delta f = -C_f \cdot \Delta f \tag{1}$$

where ρ_q is the density of quartz (2.648 g·cm^{-3}), μ_q is the shear modulus of quartz (2.947 ×1011 g ·cm·s^2), f_o is the fundamental resonance frequency of the quartz and C_f is the calibration constant (or sensitivity factor). The sensitivity factor of the resonator, C_f, was obtained by carrying out silver electroplating under constant current (chronopotentiometry) at -0.18mA·cm^{-2} on a bare quartz crystal soaked in an electrolytic solution containing 0.01 M silver nitrate and 0.1 M tetraethylammonium tetrafluoroborate in acetonitrile. The mass of the silver deposit (m) was calculated by applying Faraday's law (eq. 2), assuming a 100% faradic efficiency:

$$m = \frac{Q \cdot M_w}{n \cdot F} = \frac{I \cdot t \cdot M_w}{n \cdot F} \tag{2}$$

where Q is the charge passed through the electrode in Coulombs, I is the current in Amps, t is the time in seconds, M_w is the molecular weight of silver (107.9 g·mol^{-1}), F is the Faraday Constant (96485 C·mol^{-1}), and n is the valence number of the ion. The calibration constant C_f was then determined from the slope of Δf versus Δm curve. The value of the calibration constant used in this work is 17.5 ng·Hz^{-1}.

Chronoamperometry tests were conducted at room temperature with simultaneous recording of the quartz resonance frequency. The potential was increased from the OCV in steps of 0.1 V and held for 120 seconds at each voltage. The capacitive charge Q_c passed through the electrode was calculated by integrating the current (I) versus step duration time (t) during the potential hold (see Figure S9). The total charge Q_{total} was corrected from the contribution of the residual leakage current by subtracting the residual leakage charge $Q_{leak} = I_{leak}.t$ where t is the step duration and I_{leak} the residual stabilized current, so that $Q_c = Q_{total} - Q_{leak}$.

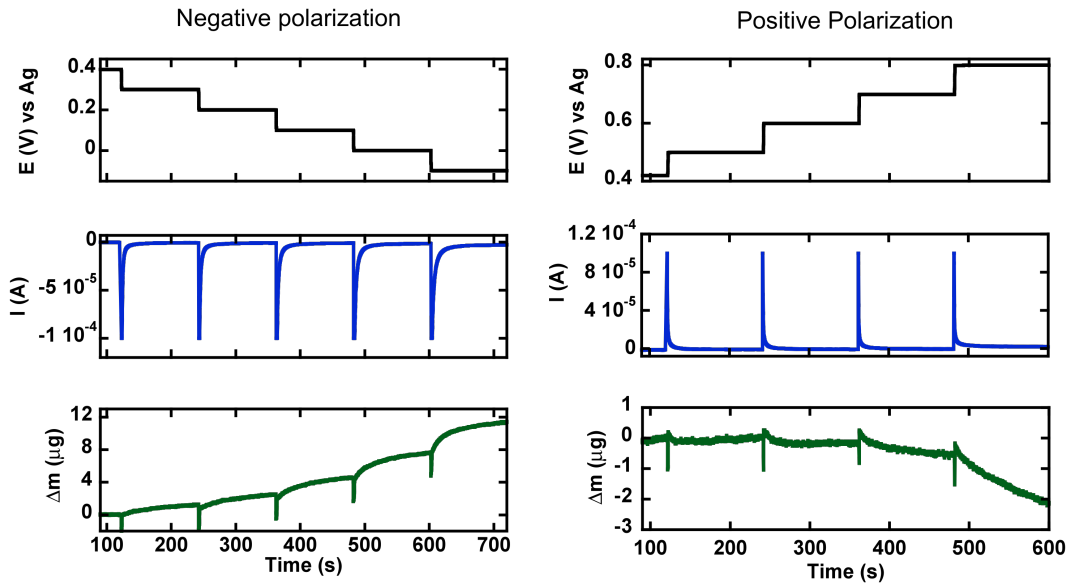

Figure S9. Electrode potentials, E, currents, I, and mass changes, Δm, of the electrode plotted as a function of time during negative (left) and positive charging (right)

Figure S9 details the chronoamperometry test on the YP50F-coated quartz crystal for positive and negative charging, showing the potential step profile (upper part), the corresponding current response (middle) and the *in situ* mass variation with time calculated using the Sauerbrey equation (equation 1).

The Sauerbrey equation can be applied under the assumption that the additional mass or film deposited on the quartz has the same acousto-elastic properties as quartz crystal, which means that the carbon deposited needs to be thin and homogenous. Therefore, the carbon loading on the quartz was kept in the range 20 – 50 μg·cm^{-2}.

An important part of EQCM analysis is based on the calculated capacitive charge which further leads to theoretical mass and the average molar weight; thus it is essential to verify that the calculated charge only originates from capacitive processes. Figure S10 shows the change of the current measured at the end of the potential steps shown in Figure S9 (after 120 s of polarisation) versus the electrode potential during the potential hold; this mimics a steady state sweep voltammetry. The current passing across an ideal capacitor is null once the equilibrium state is reached; in our case, the presence of electrolyte explains the small – but not null - steady state current (< 1 μA) between 0 and +0.7 V vs reference. However, for large polarisations of –0.1 V and +0.8 V vs reference (circles), the current increase is linked with parasitic redox reactions associated with the electrolyte. The potential range where the charge storage can be considered as fully capacitive can thus be defined between 0 and +0.7 V vs reference.

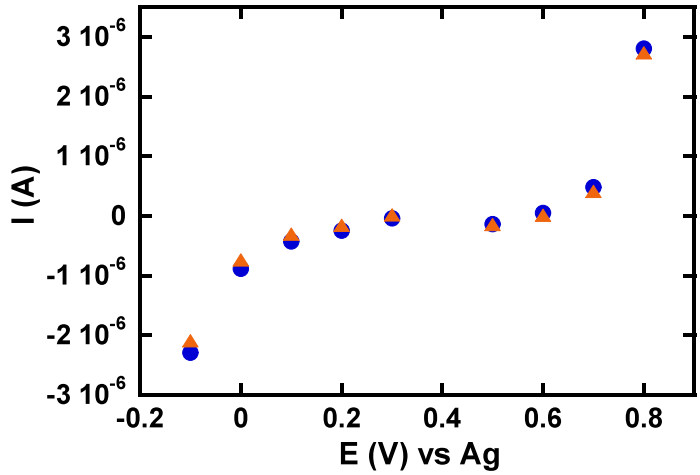

Figure S10. The average of current during the last 60 seconds or 30 seconds of each polarisation step versus potential.

Figure S11 presents the measured mass change with error bars calculated from the variation of quartz resonance frequency. These errors are small enough such that they may be neglected in the mass calculation.

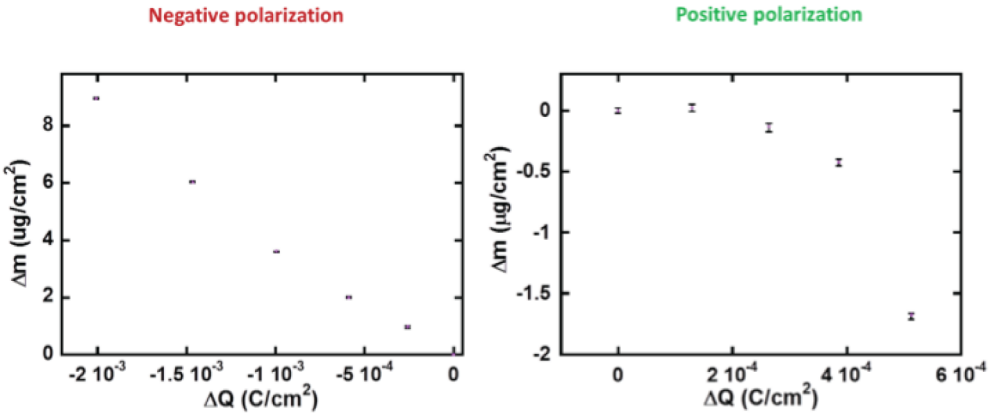

Figure S11. The measured mass change plotted as a function of charge with error bars. Errors were obtained from the variation of the frequency during measurement.

The potential of zero change (PZC) of the system was studied using a conventional three-electrode Swagelok cell: a YP-50F electrode film with a carbon loading of 7~7.5mg·cm^{-2} as working electrode, a silver wire as reference electrode (same as in EQCM set-up), and a heavy loading YP-50F electrode film (21 mg·cm^{-2}) as counter electrode. The cyclic voltammograms (at 5 mV·s^{-1}) of the full window scan in 0.75 M and 1.5 M concentration are shown in Figure S12a. A minimum capacitance is found at around 0.5 V vs reference, highlighted by red frame. Figure S12b shows the enlarge view of the highlighted part in Figure a, and second order polynomial fitting curves (black line) for both concentration are also shown. The PZCs (defined at dC/dE = 0 which means the minimum of the curves) in 0.75 M and 1.5 M concentration are both 0.49 V vs reference, close to the OCV (0.43 V vs reference), thus validating the measurements.

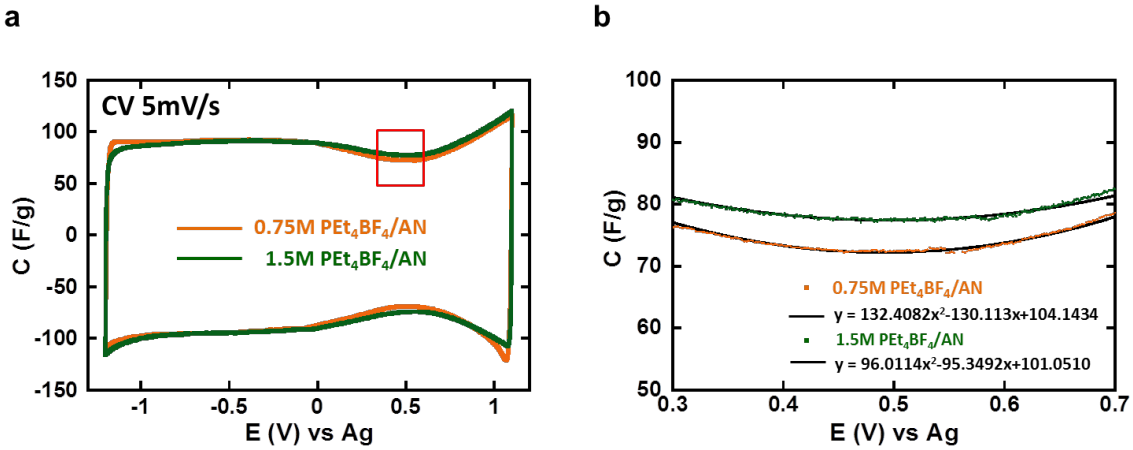

Figure S12. (a) CVs of 3-electrode Swagelok cell in 0.75 M and 1.5 M PEt_4BF_4/ACN; (b) shows the zoomed zone highlighted in (a).

9. Gas sorption experiments on YP-50F

The porosity characteristics of YP-50F carbon were obtained from an argon sorption isotherm (Fig. S13a) measured at 77 K with a Micromeritics ASAP 2020 porosimeter. The specific surface area estimated by using Brunauer-Emmett-Teller (BET) method is 1730 $m^2 \cdot g^{-1}$. The pore size distributions (PSD) were calculated from the isotherm by using Quenched Solid Density Functional Theory (QSDFT) method[S9] as shown in Fig. S13b. The calculated average pore size is 0.9 nm, and the total pore volume is 0.75 $cm^2 \cdot g^{-1}$ with 92 % of the pores smaller than 2 nm.

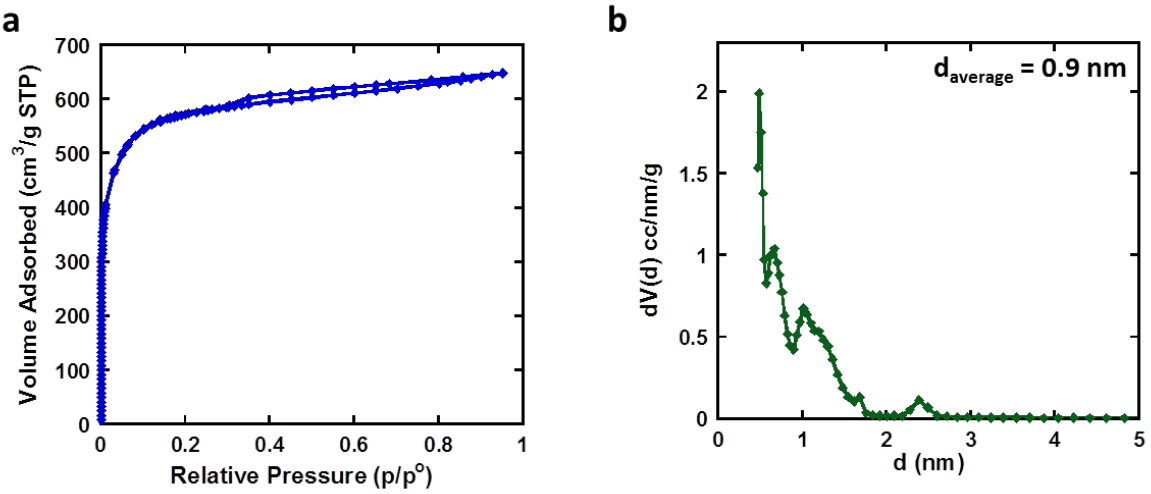

Figure S13. (a) Gas adsorption/desorption analysis of YP-50F (specific surface area ~ 1732 $m^2 \cdot g^{-1}$). (b) Pore size distribution of YP-50F powder derived from QSDFT.

References

S1. Kim, Y.-J., Masutzawa, Y., Ozaki, S., Endo, M. & Dresselhaus, M. S. PVDC-based carbon material by chemical activation and its application to nonaqueous EDLC. *J. Electrochem. Soc.*, **151**, E199-E205 (2004).

S2. Matsumoto, K., Harinaga, U., Tanaka, R., Koyama, A., Hagiwara, R. & Tsunashima, K. The structural classification of the highly disordered crystal phases of $[N_n][BF_4]$, $[N_n][PF_6]$, $[P_n][BF_4]$, and $[P_n][PF_6]$ salts (N_n^+ = tetraalkylammonium and P_n^+ = tetraalkylphosphonium). *Phys. Chem. Chem. Phys.* **16**, 23616-23626 (2014).

S3. Cory, D. G. & Ritchey, W. M. Suppression of signals from the probe in Bloch decay spectra. *J. Magn. Reson.* **80**, 128-132 (1988).

S4. Wang, H., Forse, A. C., Griffin, J. M., Trease, N. M., Trognko, L., Taberna, P.-L., Simon, P. & Grey, C. P. In situ NMR spectroscopy of supercapacitors: insight into the charge storage mechanism. *J. Am. Chem. Soc.*, **135**, 18968-18980 (2013).

S5. Massiot, D., Fayon, F., Capron, M., King, I., Le Calvé, S., Alonso, B., Durand, J.-O., Bujoli, B., Gan, Z. & Hoatson, G. Modelling one- and two-dimensional solid-state NMR spectra. *Magn. Reson. Chem.* **40**, 70-76 (2002).

S6. Deschamps, M., Gilbert, E., Azais, P., Raymundo-Piñero, E., Ammar, M., R., Simon, P., Massiot, D. & Beguin, F. Exploring electrolyte organization in supercapacitor electrodes with solid-state NMR. *Nature Mater.*, **12**, 351-358 (2013).

S7. Francke, R., Cericola, D., Kötz, R., Weingarth, D. & Waldvogel, S. R. Novel electrolytes for electrochemical double layer capacitors based on 1,1,1,3,3,3-hexafluoropropan-2-ol. *Electrochim. Acta*, **62**, 372-380 (2012).

S8. Tsai, W.-Y., Taberna, P.-L. & Simon, P. Electrochemical quartz crystal microbalance (EQCM) study of ion dynamics in nanoporous carbons. *J. Am. Chem. Soc.*, **136**, 8722-8728 (2014).

S9. Neimark, A. V., Lin, Y., Ravikovitch, P. I., Thommes, M. Quenched solid density functional theory and pore size analysis of micro-mesoporous carbons. Carbon **47**, 1617-1628 (2009).